Supporting Information

Honeycomb-like Interconnected Network of Nickel Phosphide Hetero-nanoparticles with Superior Electrochemical Performance for Supercapacitors

Shude Liu[a], *Kalimuthu Vijaya Sankar*[a], *Aniruddha Kundu*[a], *Ming Ma* [b], *Jang-Yeon Kwon*[c], *Seong Chan Jun*[a,]*

[a]School of Mechanical Engineering, Yonsei University, Seoul 120-749, South Korea

[b]Advanced Institute of Nanotechnology, Sungkyunkwan University, Suwon 440-746, South Korea

[c]School of Integrated Technology and Yonsei Institute of Convergence Technology, Yonsei University, Yeonsu-gu, Incheon 406-840, South Korea

E-mail: scj@yonsei.ac.kr *(Seong Chan Jun)*

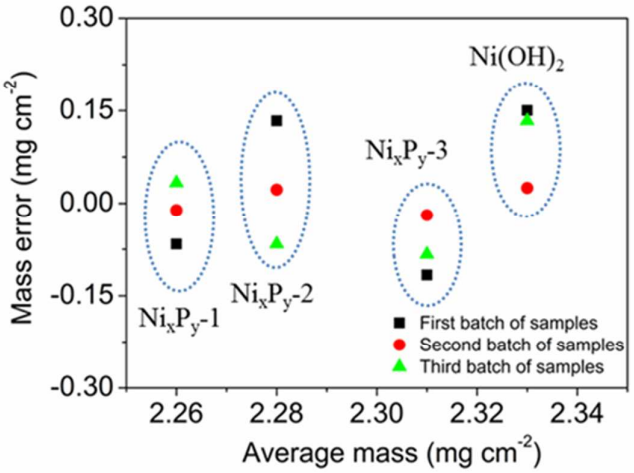

Figure S1. The mean mass loading as a function of mass error for the as-synthesized $Ni(OH)_2$, Ni_xP_y-1, Ni_xP_y-2, and Ni_xP_y-3 samples in three independent experiments.

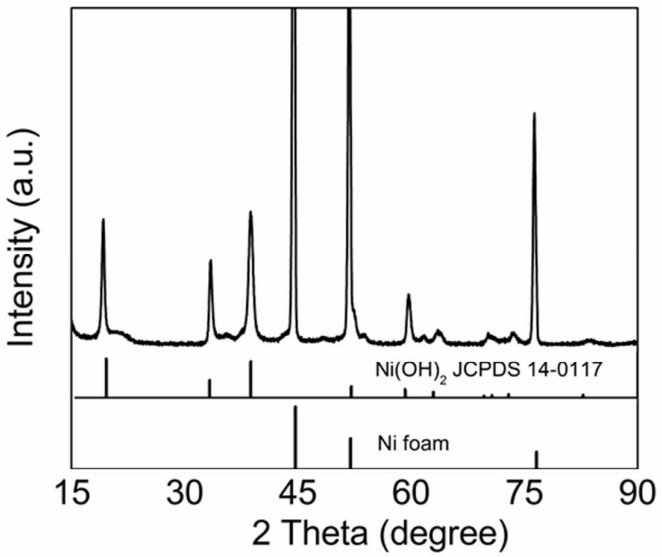

Figure S2. XRD pattern of the $Ni(OH)_2$ precursor on nickel foam.

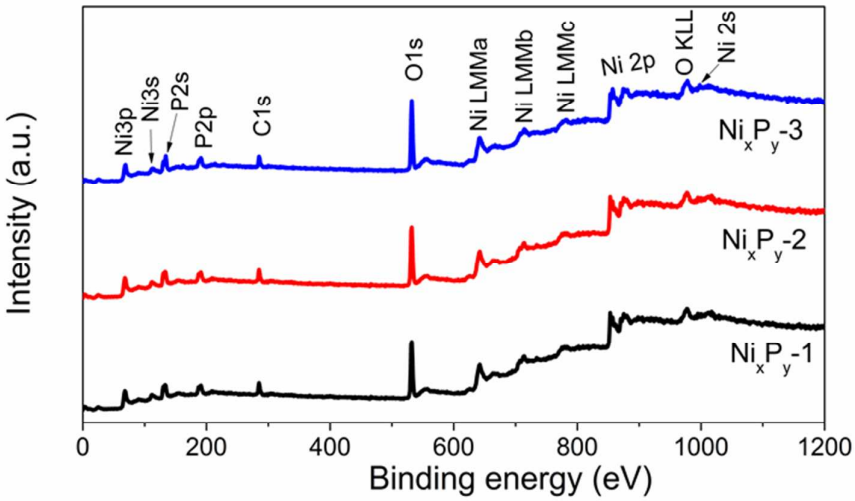

Figure S3. XPS survey spectra of Ni_xP_y-1, Ni_xP_y-2, and Ni_xP_y-3.

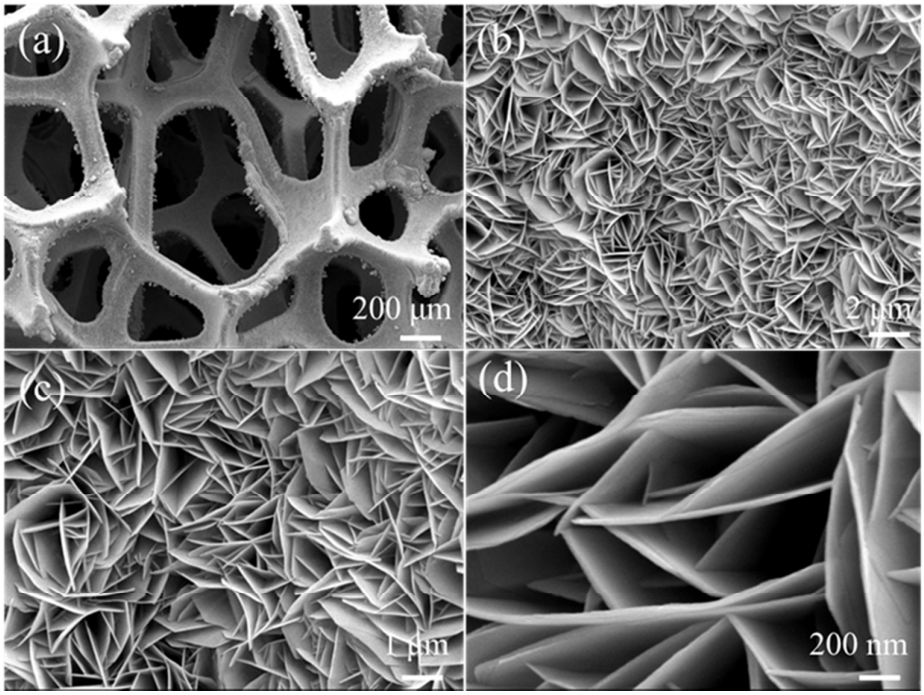

Figure S4. (a-d) SEM images of the $Ni(OH)_2$ precursor at different magnifications.

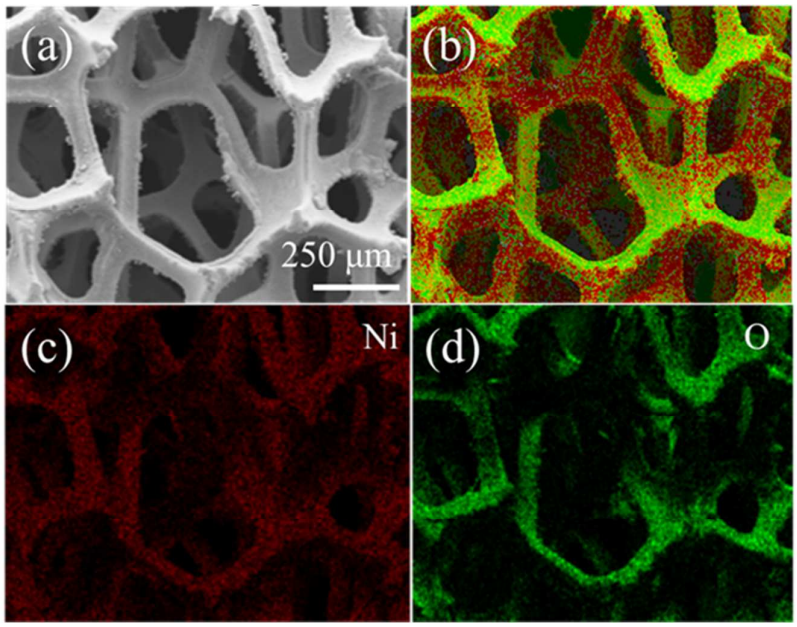

Figure S5. (a) SEM image of the $Ni(OH)_2$ precursor, and (b-d) the corresponding elemental mapping for Ni and O.

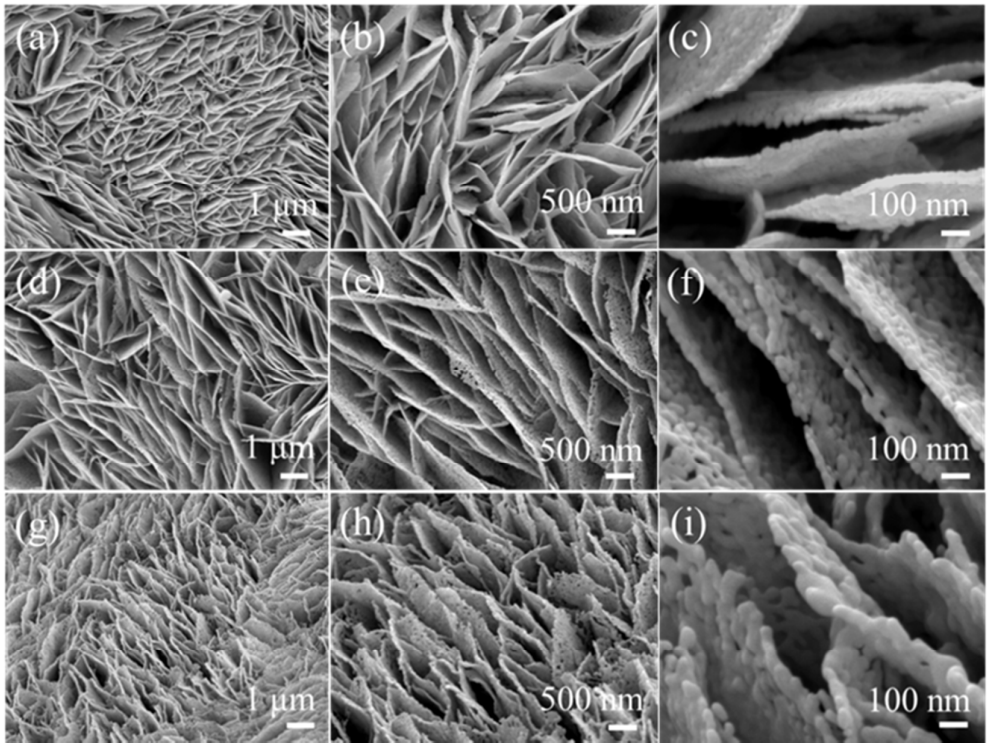

Figure S6. Typical SEM images of (a–c) Ni_xP_y-1, (d–f) Ni_xP_y-2, and (g–i) Ni_xP_y-3 at different magnifications.

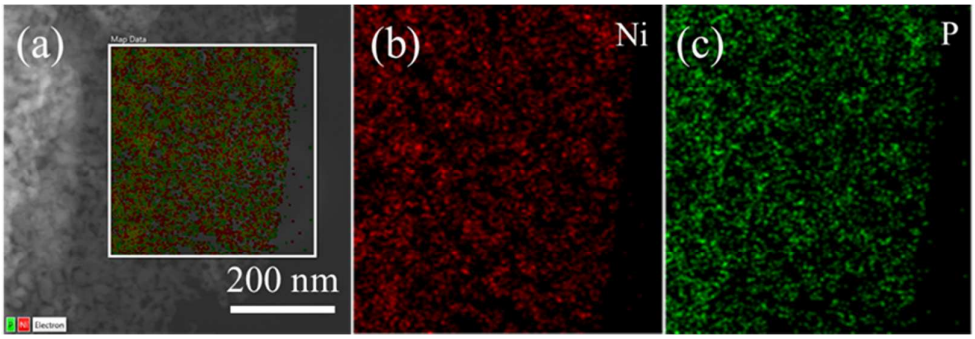

Figure S7. (a) TEM image of Ni_xP_y-1 and (b-c) corresponding elemental mapping images of Ni and P.

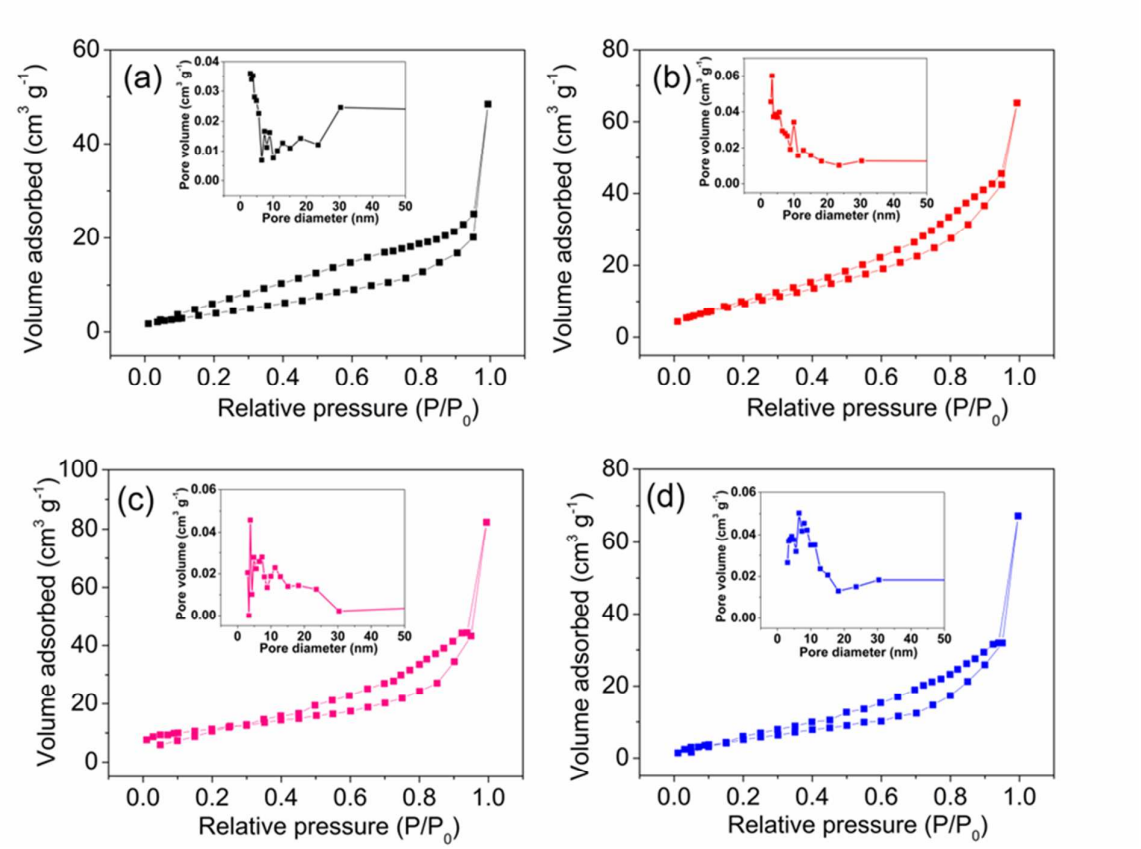

Figure S8. Nitrogen adsorption–desorption isotherms and pore size distribution curves of (a) $Ni(OH)_2$, (b) Ni_xP_y-1, (c) Ni_xP_y-2, and (d) Ni_xP_y-3 samples.

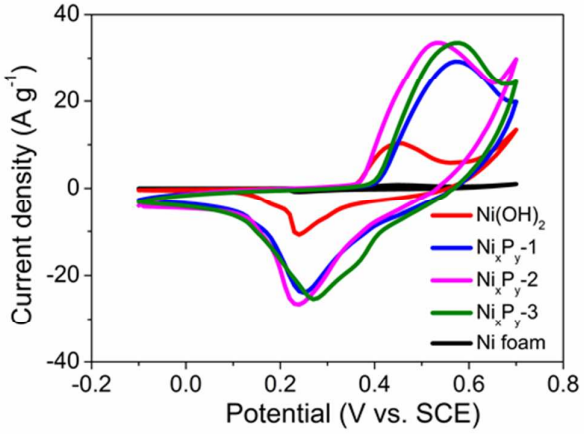

Figure S9. Comparative CV curves of pure Ni foam, $Ni(OH)_2$, Ni_xP_y-1, Ni_xP_y-2, and Ni_xP_y-3 electrodes at a scan rate of 5 mV s^{-1}.

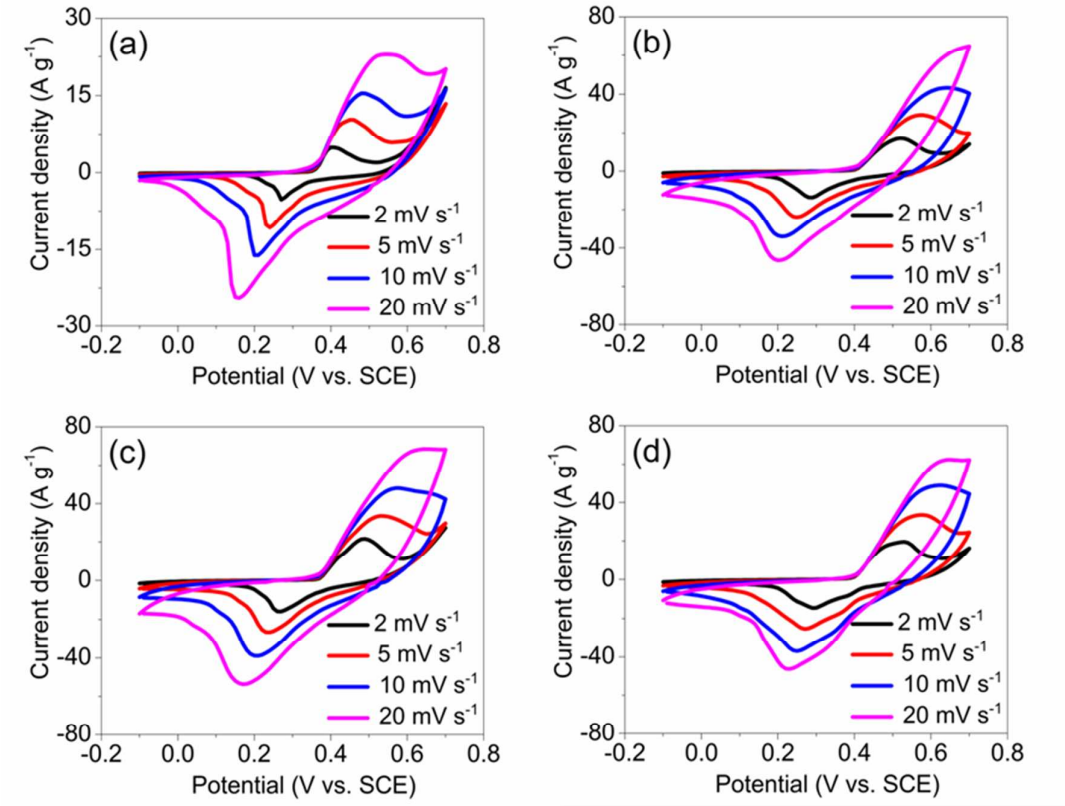

Figure S10. CV curves of (a) $Ni(OH)_2$, (b) Ni_xP_y-1, (c) Ni_xP_y-2, and (d) Ni_xP_y-3 electrodes at different scan rates.

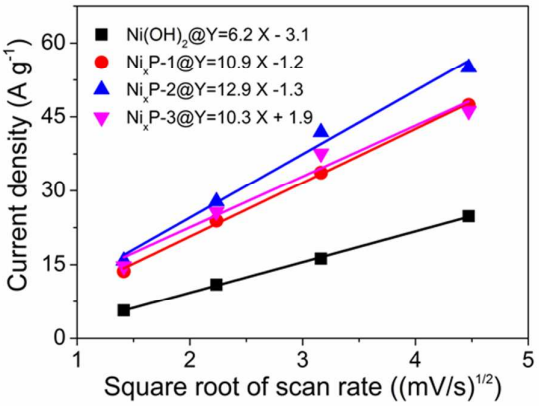

Figure S11. Dependence of the peak current density on the square root of the scan rate for the $Ni(OH)_2$, Ni_xP_y-1, Ni_xP_y-2, and Ni_xP_y-3 electrodes.

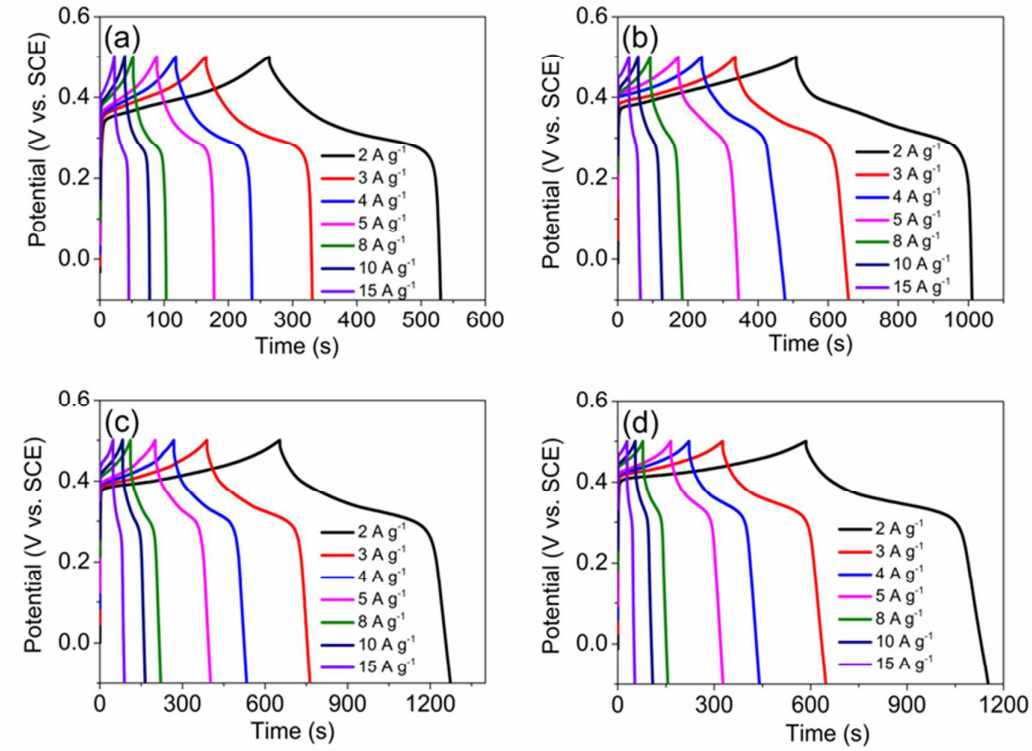

Figure S12. GCD curves of (a) $Ni(OH)_2$, (b) Ni_xP_y-1, (c) Ni_xP_y-2, and (d) Ni_xP_y-3 electrodes at various current densities.

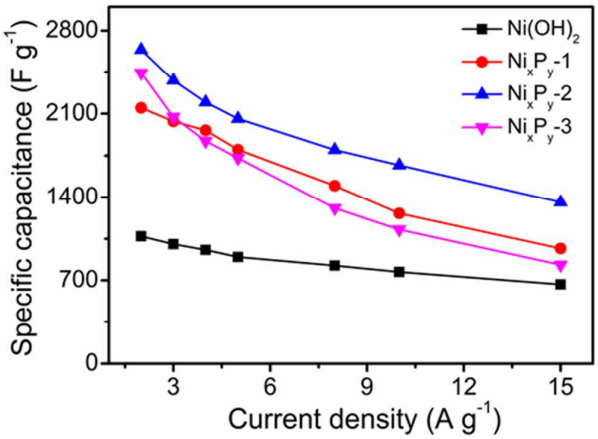

Figure S13. Comparison of specific capacitances of $Ni(OH)_2$, Ni_xP_y-1, Ni_xP_y-2, and Ni_xP_y-3 electrodes at various current densities.

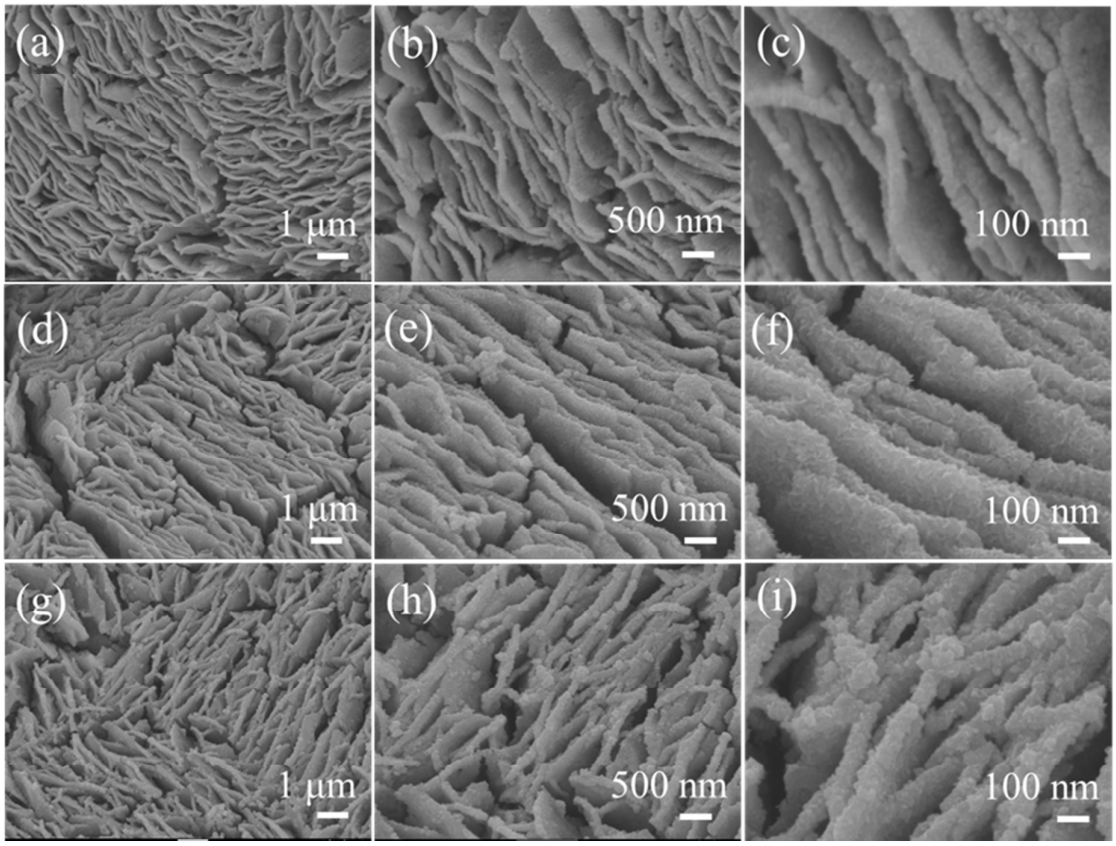

Figure S14. SEM images of (a-c) Ni_xP_y-1, (d-f) Ni_xP_y-2, and (g-i) Ni_xP_y-3 electrodes after cycling test.

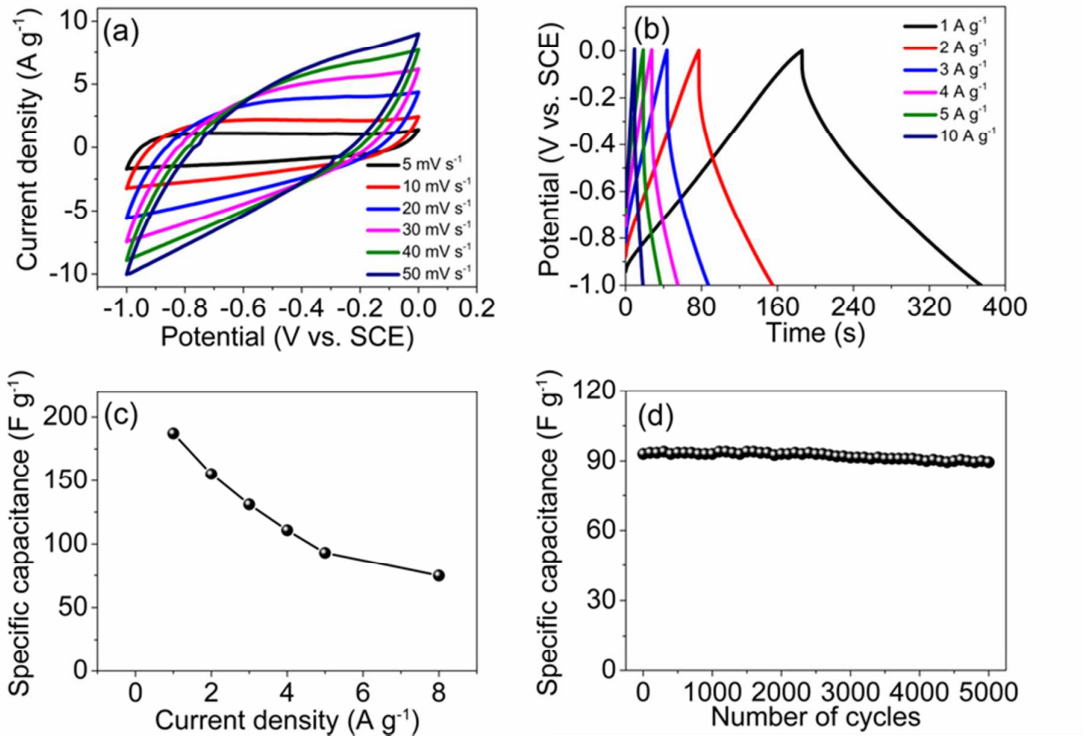

Figure S15. Three-electrode electrochemical measurements of the AC electrode in 3-M KOH: (a) CV curves at different scan rates. (b) GCD curves at different current densities. (c) Current density dependence of specific capacitance. (d) Cycling performance performed at a current density of 5 A g^{-1}.

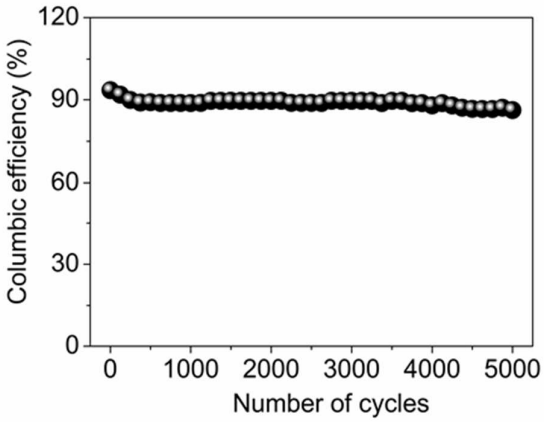

Figure S16. Coulombic efficiency of the Ni_xP_y//AC ASC device at a current density of 5 A g^{-1}.

Table S1. XPS binding energy and atoms content of Ni_xP_y composites using XPS measurement.								
Materials	Binding energy (eV)					Atom percentage (At. %)		Atomic ratio
	Ni $2p_{3/2}$		P 2p			Ni	P	Ni/P
	Ni^{2+}	$Ni^{\delta+}$	$P^{\delta-}$		PO_4^{3-}			
			P $2p_{3/2}$	P $2p_{1/2}$				
Ni_xP_y-1	856.8	853.4	129.2	130.1	133.6	21.31	14.26	1.494
Ni_xP_y-2	856.7	853.2	129.0	129.9	133.5	23.85	13.65	1.747
Ni_xP_y-3	856.5	853.1	128.9	129.8	133.4	25.61	13.27	1.930

Table S2. The percentages of Ni and P with different valences in various Ni_xP_y composites using XPS measurement.				
Materials	Ni $2p_{3/2}$		P 2p	
	$Ni^{\delta+}$	Ni^{2+}	$P^{\delta-}$	PO_4^{3-}
Ni_xP_y-1	0.411	0.330	0.436	0.564
Ni_xP_y-2	0.386	0.355	0.370	0.630
Ni_xP_y-3	0.303	0.435	0.362	0.638

Table S3. Comparison of specific capacity of reported nickel-based systems and the present Ni_xP_y hetero-nanoparticles.

Materials	Specific capacity	Current density/scan rate	Ref.
$Co_3O_4/NiCo_2O_4$ double-shelled nanocages	408 C g^{-1}	5 A g^{-1}	S1
$MnCo_2O_4$@$Ni(OH)_2$ core–shell flowers	969.3 C g^{-1}	5 A g^{-1}	S2
H-TiO_2@$Ni(OH)_2$ core–shell nanowires	1101.6 C g^{-1}	1 mV s^{-1}	S3
NiCo-LDH nanoflakes	894 C g^{-1}	2 A g^{-1}	S4
Hollow $NiCo_2O_4$ nanowalls	633.2 C g^{-1}	2.5 mA cm^{-2}	S5
Onion-like $NiCo_2S_4$ particles	508 C g^{-1}	2 A g^{-1}	S6
$NiCo_2S_4$ nanosheets/N-doped carbon	615.5 C g^{-1}	2 A g^{-1}	S7
Ni_xS_y/rGO nanoflakes	724 C g^{-1}	1 A g^{-1}	S8
Ni_xP_y hetero-nanoparticles	1272 C g^{-1}	2 A g^{-1}	Present work

Table S4. Representative fitted EIS parameters based on the experimental impedance spectra.

Materials	Fitted equivalent circuit elements							
	R_s (Ω)	R_{ct} (Ω)	C_1 (F)	CPE_T	CPE_P	W_R	W_T	W_P
$Ni(OH)_2$	0.84	12.4	0.014	0.64	0.65	30.97	0.149	0.46
Ni_xP_y-1	0.46	6.0	0.042	0.96	0.58	22.42	0.50	0.39
Ni_xP_y-2	0.43	4.6	0.058	1.06	0.51	10.15	2.42	0.41
Ni_xP_y-3	0.39	6.9	0.076	0.89	0.55	9.24	6.57	0.45

R_s: the combinational resistance of ionic resistance of electrolyte, intrinsic resistance of substrate, and contact resistance at the active material/current collector interface; R_{ct}: the charge transfer resistance; C_1: double-layer capacitance; CPE constant phase element; W is the Warburg resistance.

Table S5. Cycling stability comparison of Ni_xP_y hetero-nanoparticles with previously reported electrodes.

Materials	Capacitance retention (cycles)	Current density/Scan rate	Ref.
Co_3O_4@$Ni(OH)_2$ core–shell nanowires	76% (1000)	50 mA cm^{-2}	S9
$MnCo_2S_4$ nanowires	80.2% (6000)	20 A g^{-1}	S10
NiO/Ni_3S_2 nanosheets	82.4% (5000)	10 A g^{-1}	S11
Ni–Co sulfide nanowires	78.5 (3000)	15 mA cm^{-2}	S12
$Ni_xCo_{1-x}O$/$Ni_yCo_{2-y}P$@C hydrids	84% (3000)	10 A g^{-1}	S13
Ni_xP_y hetero-nanoparticles	90.9%(5000)	8 A g^{-1}	Present work

References

1. Hu, H.; Guan, B.; Xia, B.; Lou, X. W., Designed Formation of Co_3O_4/$NiCo_2O_4$ Double-shelled Nanocages with Enhanced Pseudocapacitive and Electrocatalytic Properties. *J. Am. Chem. Soc.* **2015,** *137*, 5590-5595.
2. Zhao, Y.; Hu, L.; Zhao, S.; Wu, L., Preparation of $MnCo_2O_4$@$Ni(OH)_2$ Core–Shell Flowers for Asymmetric Supercapacitor Materials with Ultrahigh Specific Capacitance. *Advanced Functional Materials* **2016,** *26*, 4085-4093.
3. Ke, Q.; Guan, C.; Zhang, X.; Zheng, M.; Zhang, Y. W.; Cai, Y.; Zhang, H.; Wang, J., Surface□Charge□Mediated Formation of H□TiO_2@$Ni(OH)_2$ Heterostructures for High□Performance Supercapacitors. *Adv. Mater.* **2016,** *29*, 1604164
4. Zhang, J.; Xiao, K.; Zhang, T.; Qian, G.; Wang, Y.; Feng, Y., Porous Nickel-cobalt Layered Double Hydroxide Nanoflake Array Derived from ZIF-L-Co Nanoflake Array for Battery-type Electrodes with Enhanced Energy Storage Performance. *Electrochim. Acta* **2017,** *226*, 113-120.
5. Guan, C.; Liu, X.; Ren, W.; Li, X.; Cheng, C.; Wang, J., Rational Design of Metal□Organic Framework Derived Hollow $NiCo_2O_4$ Arrays for Flexible Supercapacitor and Electrocatalysis. *Adv. Energy Mater.* **2017**, DOI: 10.1002/aenm.201602391.
6. Guan, B. Y.; Yu, L.; Wang, X.; Song, S.; Lou, X. W. D., Formation of Onion□Like $NiCo_2S_4$ Particles via Sequential Ion□Exchange for Hybrid Supercapacitors. *Adv. Mater.* **2016,** *29*, 1605051 (1-5).
7. Shen, L.; Wang, J.; Xu, G.; Li, H.; Dou, H.; Zhang, X., $NiCo_2S_4$ Nanosheets Grown on Nitrogen□Doped Carbon Foams as an Advanced Electrode for Supercapacitors. *Adv. Energy Mater.* **2015,** *5*, 1400977 (1-7)
8. Dai, S.; Zhao, B.; Qu, C.; Chen, D.; Dang, D.; Song, B.; Fu, J.; Hu, C.; Wong, C.-P.; Liu, M., Controlled Synthesis of Three-phase Ni_xS_y/rGO Nanoflake Electrodes for Hybrid Supercapacitors with High Energy and Power Density. *Nano Energy* **2017,** *33*, 522-531.
9. Tang, C.-h.; Yin, X.; Gong, H., Superior Performance Asymmetric Supercapacitors Based on a Directly Grown Commercial Mass 3D Co_3O_4@$Ni(OH)_2$ Core–shell Electrode. *ACS Appl. Mater. Interfaces* **2013,** *5*, 10574-10582.
10. Liu, S.; Jun, S. C., Hierarchical Manganese Cobalt Sulfide Core–shell Nanostructures for High-performance Asymmetric Supercapacitors. *J. Power Sources* **2017,** *342*, 629-637.
11. Liu, S.; Lee, S. C.; Patil, U. M.; Ray, C.; Sankar, K. V.; Kundu, A.; Kang, S.; Park, J. H.; Jun, S. C., Controllable Sulfuration Engineered NiO Nanosheets with Enhanced Capacitance for High Rate Supercapacitors. *J. Mater. Chem. A* **2017,** *5*, 4543-4549.
12. Li, Y.; Cao, L.; Qiao, L.; Zhou, M.; Yang, Y.; Xiao, P.; Zhang, Y., Ni–Co Sulfide Nanowires on Nickel Foam with Ultrahigh Capacitance for Asymmetric Supercapacitors. *J. Mater. Chem. A* **2014,** *2*, 6540-6548.
13. Shao, Y.; Zhao, Y.-Q.; Li, H.; Xu, C.-L., Three-Dimensional Hierarchical $Ni_xCo_{1-x}O$/$Ni_yCo_{2-y}P$@C Hybrids on Nickel Foam for Excellent Supercapacitors. *ACS Appl. Mater. Interfaces* **2016,** *8*, 35368–35376.